

Absence of charge inversion on rodlike polyelectrolytes with excess divalent counterions

Qi Wen and Jay X. Tang^{a)}

Department of Physics, Brown University, Providence, Rhode Island 02912

(Received 11 August 2004; accepted 29 September 2004)

Filamentous viruses such as fd and M13 are highly charged rodlike polyelectrolytes. In this study, we employ fd virus to test the recent prediction of charge inversion [Nguyen, Rouzina, and Shklovskii, *J. Chem. Phys.* **112**, 2562 (2000)]. Light scattering measurements show bundle formation and resolubilization of fd viruses when MgCl₂ was added from 0 to 600 mM. The effective charge of fd was studied by measuring their electrophoretic mobility using a filament tracking method uniquely suited for the system. Monte Carlo simulations were performed under canonical ensemble to predict the charge distribution around the rodlike virus. Charge inversion, which has been suggested theoretically to accompany with bundle resolubilization, was not observed in either experiments or simulations. A modified analysis of force balance is called upon to account for these new findings. © 2004 American Institute of Physics.
[DOI: 10.1063/1.1822912]

I. INTRODUCTION

In aqueous solutions, polyelectrolytes (PE) are surrounded by their counterions. These counterions mediate electrostatic interactions between the PE. The distribution of the counterions around them has been studied by applying the Counterion Condensation (CC) theory,^{1,2} Monte Carlo simulations,³ or by solving the Poisson–Boltzmann (PB) equation.⁴ The results of these theoretical studies predict that the counterions are condensed in a very thin layer around the PE surface. A short range attractive force between the like charged PE due to correlations of counterions is predicted to induce aggregation of PE.^{5–8} Experimentally, bundle formation induced by multivalent counterions has been observed for a variety of cylindrical PE such as DNA,^{9–11} F-actin,¹² and the filamentous phages M13 and fd.¹³

Aggregates of PE can redissolve when counterions are added in excess. Such a phenomenon has been shown and referred to as resolubilization.^{9,13–15} The recent theoretical treatment by Nguyen *et al.*¹⁶ provides an explanation as follows. Due to strong lateral correlations, which are underestimated in the CC theory and the PB equation, counterions condense within a thin layer surrounding the PE and form a structure similar to a Wigner Crystal on the PE surface.^{8,17} The counterions screen the charge on the PE and thus decrease the repulsion between PE. When the repulsive force is surpassed by the attractive force, aggregation occurs. At the neutralization point, the surface charge of the PE is totally neutralized and the repulsive force drops down to zero. After neutralization, the counterion charge surpasses the charge of the bare PE and the net charge of PE changes its sign. This effect is called charge inversion. The magnitude of inverted charge increases with the counterion concentration, leading to increased repulsion. When the repulsive force between PE dominates again, resolubilization is observed. Note that

terms interchangeable to charge inversion have been used in the literature, such as charge reversal⁹ and overcharging.^{18,19} To avoid mixed terminology, only the term charge inversion is used for the remaining of this paper.

Charge inversion has been observed in molecular-dynamics simulations and experiments on DNA and some other colloidal biopolymers.^{20–22} Until now, however, there is no clear experimental evidence to show that bundle resolubilization is caused by charge inversion. Therefore, we set out to directly measure the effective charge for filamentous phage fd, which undergoes bundle formation and resolubilization¹³ in a practically attainable concentration range of divalent metal ion salt, i.e., 0–600 mM MgCl₂.

In this paper, we study the effective charge of fd viruses by electrophoresis measurements and Monte Carlo simulations. Bacteriophage fd, which is very stable against changes in ionic strength and temperature, is a suitable model biopolyelectrolyte for studying changes of PE charge during bundle formation and resolubilization. For the purpose of this study, an fd virus is a charged rod with length of 880 nm and diameter of 6.6 nm. The surface of an fd virus consists of ~2700 copies of a major coat protein that covers the single stranded circular DNA at the interior. Each copy of coat protein contributes up to 4 net negative charges on the virus surface. After being screened by counterions, the effective charge Q of an fd virus in the solution is related to the electrophoretic mobility μ as $Q = \mu f$, where f is the orientation averaged hydrodynamic drag coefficient on the virus when it moves in solution.

This paper is organized in the following order. In Sec. II, we describe experiments using electrophoresis in free solution in order to detect the effective charge of fd viruses. In Sec. III, we describe the method of Monte Carlo simulations in order to predict the charge distribution around the fd virus treated as a cylinder with discrete charges distributed on the surface. In Sec. IV, we show and discuss the results of experiments and Monte Carlo simulations. In Sec. V, we de-

^{a)}Electronic mail: jay_tang@brown.edu

scribe an alternative mechanism to explain our results. In Sec. VI, we draw an overall conclusion.

II. MEASUREMENT OF EFFECTIVE CHARGE

A. Preparation of fd virus

fd virus was prepared by following the standard protocol using *E. Coli* K-38 as host bacteria, and purified by centrifuging at 130 000 g (27 k RPM using a BECKMAN SW-28 rotor) for 48 hours in CsCl gradient. The purified virus was dialyzed against a 5 mM imidazole buffer at pH 7.0. The dialysis buffer was replaced with a fresh one at least twice over 48 hours. Concentration of fd viruses is determined by measuring absorbance at 269 nm using an ultraviolet (UV) spectrophotometer (SHIMADZU UV-1601) with an extinction coefficient of $\epsilon=3.84 \text{ mg}^{-1}\cdot\text{cm}^2$. Quartz cuvettes with 1.5 ml volume and 1 cm path length are used for the concentration measurements.

The viruses were labeled by rhodamine succinimidyl ester, a kind gift from Paul A. Janmey, University of Pennsylvania Medical School, and stored in a 5 mM imidazole buffer, pH=7.0. The dye molecules were added at a low concentration on the order of micromolar and the ratio of rhodamine molecule added in order to label the virus coat protein was 1:1. The unreacted dye was removed by sedimenting the viruses and resuspending the pellet with the imidazole buffer. The extent of labeling was found to be $\sim 1:10$ of dye/coat protein molecules. Due to the low ratio of labeling, no detectable effects on the mobility of fd viruses were expected. The mobility of unlabeled fd viruses were measured by DELSA 440SX (Coulter), which is a commercial instrument for measuring zeta potential and mobility of colloids and polymers. However, we found that DELSA 440SX does not work well at extremely high salt concentrations, due to aggregates of salt and polymers generated near the electrodes.

B. Electrophoresis

A single molecule tracking method was used to measure the electrophoretic mobility of labeled fd viruses. Experiments were performed using a Nikon Eclipse E800 epifluorescence microscope with a $100\times$ oil immersion objective lens. Figure 1 shows a schematic of the assembly of a sample chamber, followed by a snapshot image of a few fd viruses. Briefly, a thin layer of $8\times 10^{-4} \text{ mg/ml}$ virus solution was confined between a cover slip and a glass slide. Two opposing sides were sealed with vacuum grease, allowing easy adjustment of sample thickness to $\sim 10 \mu\text{m}$. A drop of 3% agarose previously dissolved in the virus buffer by heating was applied on each end to seal the sample chamber and in the meantime form an electric bridge between the sample and a silver (Ag) wire electrode on either end. The combination of the Ag electrodes and the embedding gel in our experimental setup prevented the aggregation of salt, thus enabling us to measure the mobility of fd at high counterion concentrations. Both the microscope slide and the cover slip were incubated in the virus buffer with 1.5 mg/ml BSA for at least 1 h before use so that the viruses do not stick to the glass surfaces. The error caused by electro-osmotic effect is

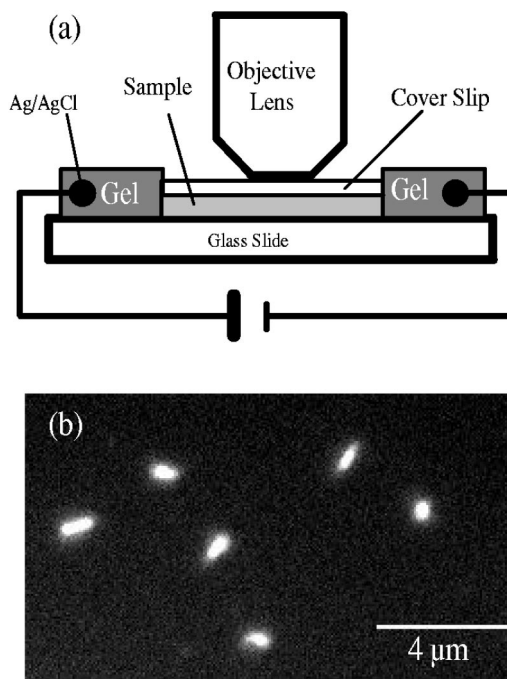


FIG. 1. (a) Schematic representation of the experimental setup for electrophoresis. The cover slip is $22\times 22 \text{ mm}$. A 5 V potential drop was applied across the sample over two Ag–AgCl electrodes each buried in a 3% agarose gel in buffer solution, thus generating an electric field of $2.27 \text{ V}\cdot\text{cm}^{-1}$. (b) A fluorescence image of single fd viruses labeled with rhodamine succinimidyl ester.

reduced by averaging the motion of the viruses over the sample thickness. A detailed assessment concerning accuracy of the measurement and how the setup was further optimized is described in a separate publication.²³

Video segments of the viruses moving under the electric field were recorded by a Cool-Snap CCD camera (Roper Scientific, New Jersey) at the rate of 5 frames per second. Image acquisition and analysis were performed using METAMORPH software (Universal Imaging Co., Indianapolis). The velocity of a single virus $v = \Delta x / \Delta t$ was obtained by tracking its trajectory, where Δt is the time interval between the first and last frame, and Δx is the displacement of the virus along the direction of the electric field over Δt . By tracking a number of trajectories, a velocity distribution for viruses at a certain counterion concentration was obtained. The velocity histogram follows a Gaussian distribution [Figs. 2(a) and 2(b)]. The average velocity is that of the directed motion under the electric field and Brownian diffusion accounts for the width of the peak. The electrophoretic mobility is determined by $\mu = \bar{v} / E$, where \bar{v} is the average velocity.

C. Static light scattering

90° static light scattering were performed using a Perkin-Elmer LS-5B luminescence spectrometer. The excitation and emission wave length were set to 365 nm (3 nm slit) and 375 nm (3 nm slit), respectively. Scattering intensity was recorded when the reading reached a steady state following the addition of a stock solution of 3 M MgCl_2 .

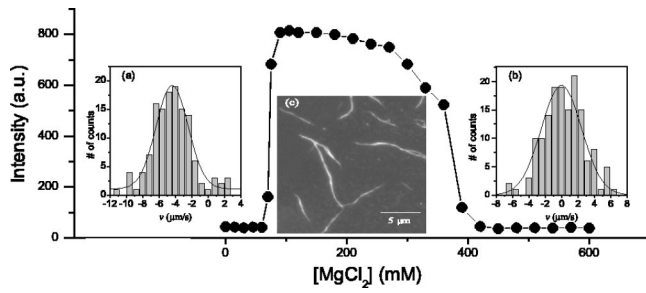


FIG. 2. Light scattering intensities for an fd virus solution following sequential additions of MgCl_2 . Insets: (a) Velocity distribution at $C_{\text{MgCl}_2} = 2 \text{ mM}$ with $\bar{v} = 3.96 \pm 0.42 \mu\text{m}\cdot\text{s}^{-1}$; (b) $C_{\text{MgCl}_2} = 600 \text{ mM}$ with $\bar{v} = 0.29 \pm 0.42 \mu\text{m}\cdot\text{s}^{-1}$, (c) A fluorescence image of the fd virus bundles taken at 100 mM MgCl_2 .

III. MONTE CARLO SIMULATIONS

By taking into account the interaction between the counterions, we use Monte Carlo (MC) simulations to study the effective charge of fd viruses at different ionic strengths. In MC simulations an fd virus was modeled as an infinitely long cylinder of diameter $d = 6.6 \text{ nm}$ with discrete negative charges on the surface of the rod. The four negative charges contributed by one major coat protein of fd form a square of 10 \AA on each side.²⁴ The packing of subunits has a periodicity of 3.3 nm along the fd axis. This model for fd is more realistic than considering the rod to be a uniformly charged line for CC theory and other analytical treatments. The solvent water was treated as a dielectric continuum with permittivity of $\epsilon = 80$ at temperature $T = 300 \text{ K}$. The mobile ions and virus charges are considered as point charges of $q_i = z_i e$, each with an effective hydrated diameter d_i .²⁴ d_i is set to be 4 \AA for all $z_i = -1$ ions including the coions and the negative charges on fd. For divalent and monovalent counterions, the values of d_i are chosen to be 6 and 5 \AA , respectively. The interaction between these spheres can be written as

$$U_{ij} = \frac{q_i q_j}{4\pi\epsilon_0\epsilon r_{ij}} + k_B T \left(\frac{d_i + d_j}{2r_{ij}} \right)^{12}, \quad (1)$$

where $r_{ij} = |r_i - r_j|$ is the distance between the ions i and j .

Periodic boundary conditions were applied in the direction of the fd axis, and the calculations have been performed in a cylindrical simulation box with length of 3.3 nm , which reflects the periodicity of subunit packing, and diameter of 40 nm , which is sufficient to enclose all counterions affected by the virus segment. Thus, only a cylindrical segment with charge of $-40e$ was included in the simulation box. The amount of divalent counterions and monovalent coions were set according to their bulk concentrations. To keep the charge neutrality of the system, 40 extra monovalent counterions were added. The total number of ions was kept constant to make an NVT ensemble for the simulation system. A Lekner summation method^{25,26} was applied to calculate the long-range electrostatic interaction from other cells. The system was pre-equilibrated by $\sim 10^6$ MC steps before collecting data for statistics. In each MC step, a mobile ion was randomly selected and then assigned a random walk. The prob-

ability of accepting a random walk follows the Metropolis Algorithm.²⁷ After pre-equilibration, a new distribution was collected after each 10^4 MC steps.

IV. RESULTS AND DISCUSSION

As shown by the light scattering data in Fig. 2, MgCl_2 induces bundle formation in the concentration range of $60 \text{ mM} < C_{\text{MgCl}_2} < 400 \text{ mM}$. A sharp increase in scattering intensity, which occurs immediately when $C_{\text{MgCl}_2} > 60 \text{ mM}$, indicates the formation of fd bundles. A sharp decrease of scattering intensity near $C_{\text{MgCl}_2} = 400 \text{ mM}$ is attributed to the resolubilization of fd bundles. In the bundle formation region, fd bundles were observed using fluorescent microscopy [see Fig. 2(c)]. Beyond that region, single viruses were detected as shown in Fig. 1(b). Since the fd bundles tend to adhere to the glass slides, filament tracking can only be performed beyond the range of bundle formation. Typical velocity distributions of single viruses are presented by histograms in Fig. 2, with MgCl_2 concentration at 2 mM (a) and 600 mM (b), respectively.

Figure 3 shows a comparison of experimental measurements, CC theory prediction, and MC simulation results on electrophoretic mobility of the fd virus. In Fig. 3(a), the fd mobility is measured at C_{MgCl_2} up to 60 mM , which is slightly lower than the threshold for bundle formation. Mobility of fd at NaCl concentrations up to 200 mM are shown in Fig. 3(b).

By considering the PE as a linear array of point charges with spacing b , Manning developed a two variable approximation to calculate the net charge q_{net} of PE and predicted the PE mobility as:¹

$$\mu = \frac{q_{\text{net}}}{900\pi\eta b} |\ln \kappa b|, \quad (2)$$

where κ is the inverse of the Debye screening length, and η is the solution viscosity. At low MgCl_2 concentrations, the theoretical prediction agrees well with the experimental results. However, when $C_{\text{MgCl}_2} > 20 \text{ mM}$ experimental data show lower mobilities than predicted. Because the viscosity of the medium is practically constant when $C_{\text{MgCl}_2} < 60 \text{ mM}$,²⁸ a lower mobility indicates a smaller net charge. Thus, there are more counterions condensed around the viruses than theoretically predicted. The CC theory does not fit well to the experimental data taken at high divalent counterion concentrations. This marked discrepancy is due to the fact that the theory ignores the correlations between counterions, the effect of which becomes stronger with increasing counterion concentrations.¹⁶

By taking into account the interaction between counterions, MC simulations yield results consistent with the experimental data. In the MC simulations, values of integrated charge Q_I , which is normalized by the surface charge Q_S of a bare virus around the viruses at different counterion concentrations, were calculated. The results are shown in Fig. 4. Taking the value of the integrated charge at the distance of 1.80 nm (3 times the diameter for divalent counterions) away from the rod surface as the effective charge of fd virus, we

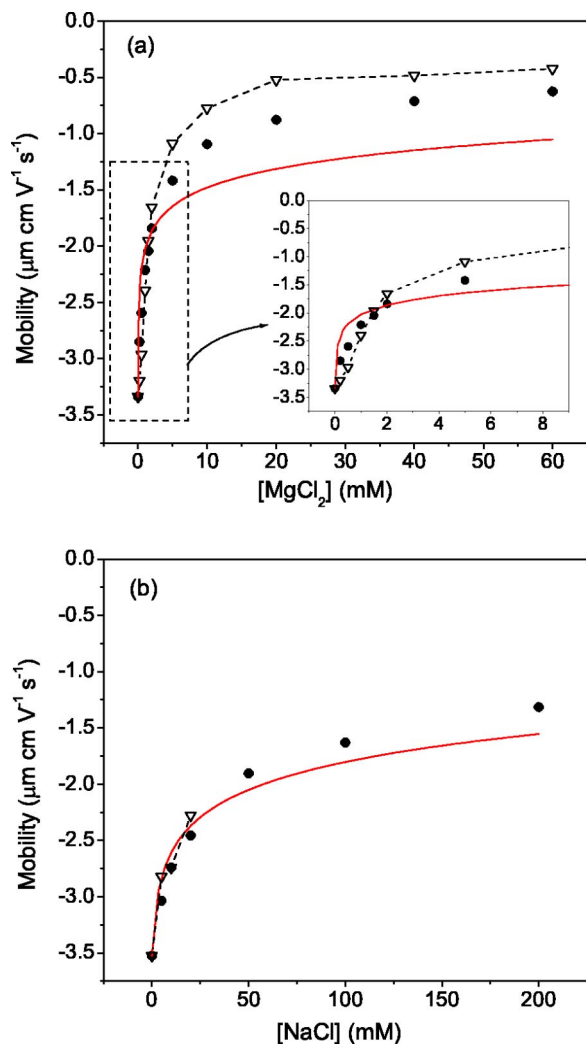


FIG. 3. Comparison of the electrophoretic mobility data with predictions from CC theory and MC simulations. Solid line is prediction by Manning CC theory. Filled circles are experimental results. Empty triangles are Monte Carlo simulation results. (a) Mobility values at $[\text{MgCl}_2] \leq 60$ mM. A detailed view of $[\text{MgCl}_2] \leq 10$ mM is shown in the inset. (b) Mobility values at $[\text{NaCl}]$ up to 200 mM.

calculated the mobility of fd using $\mu = (Q/Q_0)\mu_0$, where Q_0 is the effective charge of the rod at $C_{\text{MgCl}_2} = 0$, and $\mu_0 = -3.34 \mu\text{m} \cdot \text{cm} \cdot \text{V}^{-1} \cdot \text{s}^{-1}$ is the mobility of fd virus measured by experiments.

Both simulation and experimental results indicate that bundle formation occurs prior to the total neutralization of the fd charge. At $C_{\text{MgCl}_2} = 60$ mM, which is the threshold concentration for bundle formation, $\mu = -0.63 \pm 0.18 \mu\text{m} \cdot \text{cm} \cdot \text{V}^{-1} \cdot \text{s}^{-1}$. The mobility bears the same sign as that for $C_{\text{MgCl}_2} = 0$ mM but its magnitude is reduced by 82%. In contrast, up to 200 mM NaCl causes only a 67% mobility decrease, which is not large enough to induce bundle formation.^{12,13} It could be concluded that aggregation of PE occurs when counterions partially neutralize the fd charge to such a large extent that the repulsion between like charged viruses is surpassed by the attractive force.

The attractive force, which causes bundle formation, is induced by correlated nonuniform counterion distributions near the PE surfaces.^{6-8,29-31} Two possible mechanisms lead-

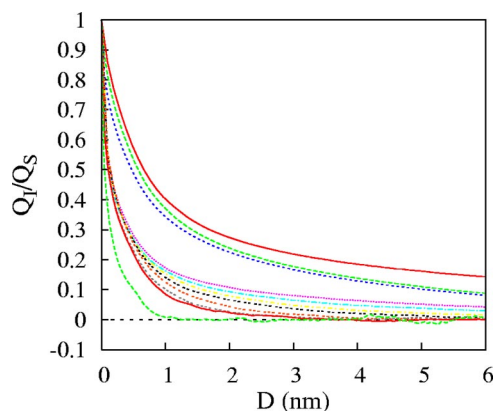


FIG. 4. Distribution of the integrated charge as a function of D , the distance from the virus surface. Q_I is the integrated charge at D . Q_s is the surface charge of a bare fd virus. Curves from top to bottom represent $C_{\text{MgCl}_2} = 0, 0.2, 0.5, 1, 2, 5, 10, 20, 40, 60,$ and 600 mM, respectively. Note that the predicted values of the normalized effective charge remain above the dashed line drawn at $Q_I = 0$, indicating no charge inversion.

ing to a nonuniform distribution of counterions along the longitudinal axis of PE have been suggested: (i) Thermal fluctuation of counterions on the PE surface causes instantaneous variations in charge distribution along the PE axis, which intercorrelate on parallel PEs and lead to an attractive force.^{7,29,30} In the thermal fluctuation picture the attractive force increases with temperature;⁶ (ii) counterions may be longitudinally arranged on PE surfaces, forming a Wigner crystal. The arrangement of the counterions on two opposing PEs correlate to induce attractive force.^{6,8} In the Wigner crystal picture, Grønbech-Jensen *et al.* show that the attractive force decreases with temperature (as T^{-2}).⁶ The Wigner crystal can survive to ambient temperature and has been observed in experiments, in which one-dimensional (1D) charge density waves along PE axis in actin bundles have been observed using x-ray scattering.³¹ Therefore, the short range spatial correlation in counterion positions is primarily responsible for the attractive interaction.

At $C_{\text{MgCl}_2} = 450$ and 600 mM, which are above the threshold concentration for resolubilization, the virus mobility was measured to be practically zero (0.11 ± 0.18 and $0.13 \pm 0.18 \mu\text{m} \cdot \text{cm} \cdot \text{V}^{-1} \cdot \text{s}^{-1}$, respectively). The results of MC simulations at the divalent counterion concentration of 600 mM only show charge neutralization when the distance from the rod surface is larger than 1.2 nm. No charge inversion, which would yield positive electrophoretic mobility, was observed.

V. MECHANISMS FOR BUNDLE RESOLUBILIZATION

Most theoretical works on resolubilization give results of charge inversion. The charge inversion theory of Nguyen and Shklovskii, as introduced in Sec. I, can be successfully applied to colloidal particles with their counterions.²¹ Based on an Ising-type mean-field model, Yu and Carlsson developed a treatment to explain the counterion induced bundle formation and resolubilization of F-actin.³² In their calculations, F-actin is also expected to be charge inverted when the counterion concentration is increased to a few hundred mM.³³ However,

our experimental results on fd show no charge inversion. Thus, those theoretical predictions for resolubilization based on the concept of charge inversion do not hold for the system of fd with the presence of divalent counterions. Therefore, an alternative theory is needed, which predicts both bundle formation and resolubilization for a system of charged rods and their counterions.

The calculations of Ha and Liu,^{7,34} in which charged rods are simplified as linear charges screened by mobile counterions provide partial theoretical explanation for the resolubilization without invoking charge inversion. These authors argue that the origin of an overall repulsive interaction may be attributed to the screening effect of the added salt. At extremely high ionic strengths, the added salt screens the attractive force more effectively than the repulsive force, since the screening length for the attractive force is half of that for the repulsive force.³⁰ Following Eq. (5) of Ref. 34, at $C_{\text{MgCl}_2} = 600 \text{ mM}$, a net repulsive interaction with free energy of $6 \times 10^{-4} k_B T$ per surface charge is obtained and the effective charge of the rod is $Q = 0.028 Q_0$ per surface charge. Because each virus carries on the order of 10 000 surface charges, the barrier is about a few $k_B T$ per virus, which is high enough for the resolubilization to occur.

VI. CONCLUSION

In summary, we studied the effects of counterions on the surface charge of fd viruses by measuring their electrophoretic mobility and by using Monte Carlo simulations. The counterions screen the repulsive force by reducing the effective charge of the viruses. Bundles form when the viruses are still negatively charged, albeit more weakly so. The fd mobility measurements provide a direct evidence that the charge inversion is not a prerequisite for the resolubilization of fd virus bundles. Our finding is tentatively explained by an estimate following a recent theoretical work of Ha and Liu.³⁴ More accurate numerical simulations or analytical treatments on the interactions between the rods are needed, however, for further understanding of the resolubilization mechanism.

ACKNOWLEDGMENTS

We thank co-workers Karim Addas and Guanglai Li for their assistance with the experiments. We acknowledge helpful communications with A. E. Carlsson, B.-Y. Ha, P. A. Janmey, A. Lyubartsev, and B. I. Shklovskii. We are grateful to Professor Paul Dubin of Indiana University Purdue Uni-

versity of Indianapolis (IUPUI) for extensive use of the DELSA 440SX in his laboratory. This work was supported by NSF DMR0405156 and NIH R01 HL67286.

- ¹G. S. Manning, *Q. Rev. Biophys.* **2**, 180 (1978).
- ²G. S. Manning and J. Ray, *J. Biomol. Struct. Dyn.* **16**, 461 (1998).
- ³P. Mills, C. F. Anderson, and M. T. Record, Jr., *J. Phys. Chem.* **89**, 3984 (1985).
- ⁴U. Mohanty, B. W. Ninham, and I. Oppenheim, *Proc. Natl. Acad. Sci. U.S.A.* **93**, 4342 (1996).
- ⁵I. Rouzina and V. A. Bloomfield, *J. Phys. Chem.* **100**, 9977 (1996).
- ⁶N. Grønbech-Jensen, R. J. Mashl, R. F. Bruinsma, and W. M. Gelbart, *Phys. Rev. Lett.* **78**, 2477 (1997).
- ⁷B.-Y. Ha and A. J. Liu, *Phys. Rev. Lett.* **79**, 1289 (1997).
- ⁸B. I. Shklovskii, *Phys. Rev. Lett.* **82**, 3268 (1999).
- ⁹J. Pelta, F. Livolant, and J.-L. Sikorav, *J. Biol. Chem.* **271**, 5656 (1996).
- ¹⁰V. A. Bloomfield, *Biopolymers* **44**, 269 (1997).
- ¹¹V. A. Bloomfield, *Biopolymers* **31**, 1471 (1991).
- ¹²J. X. Tang, S. Wong, P. T. Tran, and P. A. Janmey, *Ber. Bunsenges. Phys. Chem.* **100**, 796 (1996).
- ¹³J. X. Tang, P. A. Janmey, A. Lyubartsev, and L. Nordenskiöld, *Biophys. J.* **83**, 566 (2002).
- ¹⁴E. Raspond, M. O. de la Cruz, J. L. Sikorav, and F. Livolant, *Biophys. J.* **74**, 381 (1998).
- ¹⁵M. Saminathan, T. Antony, A. Shirahata, L. H. Sigal, T. Thomas, and T. J. Thomas, *Biochemistry* **38**, 3821 (1999).
- ¹⁶T. T. Nguyen, I. Rouzina, and B. Shklovskii, *J. Chem. Phys.* **112**, 2562 (2000).
- ¹⁷A. Y. Grosberg, T. T. Nguyen, and B. I. Shklovskii, *Phys. Rev. Lett.* **78**, 2477 (1997).
- ¹⁸E. Allahyarov, G. Gompper, and H. Löwen, *Phys. Rev. E* **68**, 061903 (2003).
- ¹⁹E. Allahyarov, G. Gompper, and H. Löwen, *Phys. Rev. E* **69**, 041904 (2004).
- ²⁰M. Tanaka, *Phys. Rev. E* **68**, 061501 (2003).
- ²¹E. Raspond, I. Chaperon, A. Leforestie, and F. Livolant, *Biophys. J.* **77**, 1547 (1999).
- ²²A. Y. Grosberg, T. T. Nguyen, and B. I. Shklovskii, *Rev. Mod. Phys.* **74**, 329 (2002).
- ²³G. Li, Q. Wen, and J. Tang (unpublished).
- ²⁴A. P. Lyubartsev, J. X. Tang, P. A. Janmey, and L. Nordenskiöld, *Phys. Rev. Lett.* **81**, 5465 (1998).
- ²⁵J. Lekner, *Physica A* **176**, 485 (1991).
- ²⁶N. Grønbech-Jensen, G. Hummer, and K. M. Beardmore, *Mol. Phys.* **92**, 941 (1997).
- ²⁷N. Metropolis, A. Rosenbluth, M. R. A. Teller, and E. Teller, *J. Chem. Phys.* **21**, 1087 (1953).
- ²⁸D. R. Lide, *Handbook of Chem. and Phys.* **82**, 8 (2002).
- ²⁹R. Golestanian and T. B. Liverpool, *Phys. Rev. E* **66**, 051802 (2002).
- ³⁰J. L. Barrat and J. F. Joanny, *Adv. Chem. Phys.* **94**, 1 (1996).
- ³¹T. E. Angelini, H. Liang, W. Wriggers, and G. C. Wong, *Proc. Natl. Acad. Sci. U.S.A.* **100**, 8634 (2003).
- ³²X. Yu and A. Carlsson, *Biophys. J.* **85**, 3532 (2003).
- ³³X. Yu and A. Carlsson (personal communication).
- ³⁴B.-Y. Ha and A. J. Liu, *Phys. Rev. Lett.* **81**, 1011 (1998).